Hindawi
Advances in Civil Engineering
Volume 2021, Article ID 5595372, 13 pages
https://doi.org/10.1155/2021/5595372

Research Article

Mining-Induced Redistribution of the Abnormal Stress under the Close Bearing Coal Pillar for Entry Design

Xudong Liu,[1] Wenlong Shen,[1,2,3] Jianbiao Bai,[1,4] Rui Wang,[1] Jizhong Kang,[1] and Xiangyu Wang[1]

[1]*Key Laboratory of Deep Coal Resource Mining Ministry of Education, State Key Laboratory of Coal Resources and Safe Mining, China University of Mining & Technology, Xuzhou 221116, Jiangsu, China*
[2]*School of Energy Science and Engineering, Henan Polytechnic University, Jiaozuo 454000, Henan, China*
[3]*Collaborative Innovation Center of Coal Work Safety and Clean High Efficiency Utilization, Jiaozuo 454000, China*
[4]*College of Mining Engineering and Geology, Xinjiang Institute of Engineering, Urumqi 830023, China*

Correspondence should be addressed to Wenlong Shen; shenwenlong.888@163.com and Jianbiao Bai; baijianbiao_cumt@163.com

Received 22 February 2021; Revised 8 March 2021; Accepted 23 March 2021; Published 8 April 2021

Academic Editor: Zhijie Zhu

Underground space is vulnerable to large deformation influenced by the abnormal stress induced by the bearing coal pillar. A numerical simulation model was established to determine the redistribution of the abnormal stress induced by the mining activities. The double-yield model, the strain softening model, the interface model, and the Mohr–Coulomb model were determined to simulate the gob compaction effect, the pillar strength reduction effect, the structure plane discontinuity effect, and the rock mechanical behavior, respectively. This numerical simulation model is reliable to predict the abnormal stress under the bearing coal pillar by the comparison of the abutment stress from this model and the existing theoretical model as well as the entry roof surface displacement from this model and the field measuring method. The results from the validated numerical model indicate that the abnormal stress including stress concentration coefficient, stress gradient, and lateral pressure coefficient will redistribute to another state that the stress concentration coefficient and stress gradient increase gradually and then decrease, and the lateral pressure coefficient decreases gradually, then increases, and finally decreases sharply with the approach of the mining working face. Their maximum increasing rates are calculated as 121.05%, 198.56%, and 236.82%, respectively. This predicted mining-induced redistribution of the abnormal stress is available for designing the underground entry layout in the determination of the entry position, determination of the driving operation time, mining disturbing range warning, and the prediction of the strengthening support area.

1. Introduction

Coal as one of the widely used energy resources in recent years will be used to accelerate the social development for a long time in the future. Its generation conditions play a significant role in the underground mining engineering, which are divided into shallow-buried condition, deep-buried condition, thin seam, thick seam, horizontal seam, dip seam, soft seam, hard seam, single seam, and multiple seams [1]. The underground mining engineering has to be carried out in multiple coal seams with the growth of the mining intensity and the reduction of the coal resources [2]. Numerous coal pillars will be left to bear the overburdens, and the generated abutment stress will transfer into the close and unworked out coal seams, which generates an abnormal stress condition in the unworked out coal seam and threatens the stability of the underground entry, especially for the condition influenced by the mining operation of the longwall mining working face [3].

The precious achievements mainly concentrate on the stress distribution under the bearing coal pillar, which ignore the abnormal characteristics especially for the disturbing effect of the mining operation [4–7]. The CVISC rheological constitutive model was used to simulate the long-term creep behavior of the entry rock under bearing coal pillar and revealed that the stress concentration was not

large enough to damage this creep behavior rock under shallow-buried conditions [8]. The numerical simulation model with the Mohr–Coulomb criterion was used to reveal the distribution of the abutment stress around the mining working face near the bearing coal pillar and design the entry position for a special case [9]. However, this achievement just concentrates on the mining operation in one thick coal seam, which did not consider the lithology difference, gob compaction effect, and the pillar strength reduction effect. Deviatoric stress evolution under the bearing coal pillar was determined to predict the plastic zone around the entry and design its support technology with the advancement of the deviatoric stress-induced failure criterion [10]. However, this deviatoric stress ignores the volumetric strain of rock materials, which did not agree with the reality.

Entry layout has been widely used to protect this kind of entry from stress concentration disaster [11–13]. The pressure diffusion angle was used to design the entry layout below the bearing coal pillar, and the stress was divided into stress reducing area and stress increasing area, which ignored the influence of the abnormal stress condition [14]. Eight meters wide coal pillar was determined to layout the gob side entry under bearing coal pillar by the criterion of minimum plastic failure zone in the entry roof, which is a significant attempt for that geological and engineering condition [15]. Under the failure analysis of a typical case, it is demonstrated that the entry under the bearing coal pillar is vulnerable to stress concentration, and this entry can be arranged at a relative reasonable position, but this analysis ignored the influence of the abnormal stress [16]. Pressure bulb theory was used to determine the reasonable entry position at 71 m or 156 m away from the bearing coal pillar based on the maximum principle stress or the maximum shear stress predicted by a numerical simulation model, which is much larger than 30 m used in reality [17].

In this work, a numerical simulation model was established to reveal the mining-induced redistribution of the abnormal stress under the bearing coal pillar, which was validated by a theoretical model and a measuring method. After that, this validated model was used to predict the redistribution of the abnormal stress both in front and lateral sides of the mining working face. These predicted results are available for designing the entry layout under the bearing coal pillar with the disturbance of the mining operation. In fact, the abnormal stress is the stress state of rock below the bearing coal pillar, which is illustrated by the three key parameters of stress concentration coefficient, stress gradient, and lateral pressure coefficient.

2. Materials and Methods

Several factors were taken into consideration to make the numerical simulation model reliable such as the gob compaction effect, the pillar strength reduction effect, the structure plane discontinuity effect, and the rock mechanical behavior, respectively. This numerical model was established under the condition of the process as shown in Figure 1. The detailed process is demonstrated as the following section.

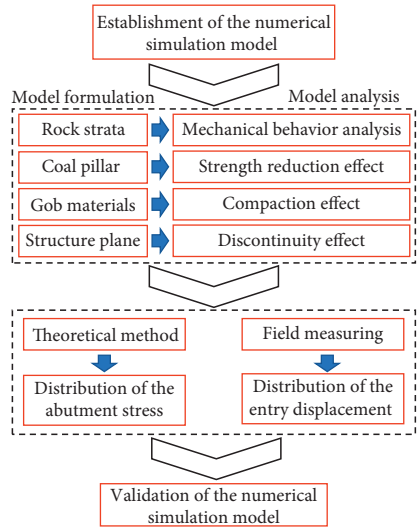

Figure 1: Formation process of the numerical simulation model.

2.1. Numerical Simulation Model

2.1.1. Mohr–Coulomb Model for Rock Strata. Rock materials will experience elastic deformation and plastic damage influenced with loadings, which can be simulated by the Mohr–Coulomb model expressed as equation (1) [18–20]. The rock materials are concentrated on a typical case from Xinrui coal mine in China. There are many bearing coal pillars left in coal seam 4 which was mined out several years ago. The entries of coal seam 5 will be influenced by these kinds of bearing coal pillars [3]. The average interlayer spacing between coal seams 4 and 5 is determined as 3.25 m, and the average stratigraphic dip angle is revealed as 6°. The detailed geological and engineering conditions are given in Table 1.

$$f = \sigma_1 - \sigma_3 \frac{(1 + \sin \varphi)}{(1 - \sin \varphi)} + 2c \sqrt{\frac{(1 + \sin \varphi)}{(1 - \sin \varphi)}}, \quad (1)$$

where f is the failure criterion; σ_1 and σ_3 are the principal stresses; φ is the frictional angle; c is the cohesion.

2.1.2. Strain Softening Model for Coal Pillar. One of the horizontal stresses is in the state of relief in the coal pillar due to the fact that both sides of the coal pillar are the workout area, and no objects apply stress along the rib sides of the coal pillar. However, the other horizontal stress is relatively stable, and the vertical stress varies, usually increases influenced by the abutment stress. Under the condition of the ultimate balance theory and plastic bearing characteristics [21, 22], the shallow coal bodies of the coal pillar will change into plastic deformation from elastic deformation with the increases of the vertical stress, which will result in the strength reduction of the coal pillar. And this mechanical behavior of the coal pillar has been demonstrated and described with the strain softening model [23–26]. The strength will decline rather than keeping stable after the coal is damaged. The reduction law of the strength parameters is

Table 1: Geological and engineering conditions of the research object.

Lithology	Thickness (m)	Bulk modulus (GPa)	Shear modulus (GPa)	Friction (°)	Cohesion (MPa)	Tension (MPa)
Sandstone	12.30	14.88	10.25	38	5.0	4.0
Coal seam 3	0.70	5.56	2.27	16	2.0	0.5
Mudstone	9.00	0.58	0.27	36	4.4	1.45
Coal seam 4	1.70	2.78	1.14	16	0.3	0.2
Sandy mudstone	3.25	8.33	4.76	35	3.5	0.65
Coal seam 5	2.76	5.56	2.27	9.5	1.6	0.5
Sandy mudstone	4.80	8.33	4.76	36	6.75	1.4
Sandstone	2.40	14.88	10.25	38	7.0	5.0
Mudstone	6.60	6.67	3.08	36	4.4	1.45
Limestone	4.50	23.02	11.24	42	10.0	8.0

Table 2: Parameters of the strain softening model for coal pillar.

Plastic strain	0	0.01	0.02	...	0.5
Friction angle (°)	9.5	8.5	7.5	...	7.5
Cohesion (MPa)	1.6	1.2	0.9	...	0.9

given in Table 2 by the method of trial-and-error in terms of the peak vertical stress (18.8 MPa) and the width of plastic zone (5.5 m) beside the gob.

2.1.3. Double-Yield Model for Gob Material. The null model is widely used to simulate the gob material in longwall mining around the world [27], which ignored the consolidation of the caved rock strata. With the improvement of the numerical simulation technology and equivalence principle, the double-yield model gradually plays the main role to simulate the mechanical behavior of the gob material instead of the null model [28]. The key parameter is the cap pressure which usually follows a piecewise-linear law with the increases of the volumetric plastic strain. Salamon's model [29] (equation (2)) is used to calculate this cap pressure, and the result is given in Table 3. The basic properties of the double-yield model used for the gob material are given in Table 4.

$$\sigma = \frac{10.39\sigma_c^{1.042}h_{\text{cav}}^{7.7}h_m\varepsilon}{(h_{\text{cav}}+h_m)^{7.7}\left[h_m-(h_{\text{cav}}+h_m)\varepsilon\right]}, \tag{2}$$

where σ is the cap pressure; ε is the plastic strain; σ_c is the in situ vertical stress; h_{cav} is the caving height; h_m is the mining height.

2.1.4. Interface Model for Structure Plane. Coal-bearing strata belong to sedimentary strata which contain structure plane located between coal seam and rock strata [30]. This kind of structure plane is so weak compared with the coal and rock materials that the separation and slippage damage always generate along this structure plane. The predicted results cannot be used to guide the operation of the engineering unless this structure plane is considered in the numerical simulation model [31]. The interface element follows the Mohr–Coulomb failure criterion illustrated as equation (3) [32]. When the shear stress is larger than the shear strength, the slippage will generate along the interface, and when the normal deformation capability is not consistent for strata, the separation will generate along the interface. Jaeger and Cook's model [33] shown in equation (4) can be used to determine the parameters of the structure plane, and the results are illustrated in Table 5. The uniaxial compression strength of the structure plane is determined as 0.17 MPa.

$$F_{\text{smax}} = c_sA + \tan\varphi_s(F_n - pA), \tag{3}$$

where F_{smax} is the ultimate shear force; c_s is the cohesion of the interface; φ_s is the friction angle of the interface; A is the representative area touched with the interface node; F_n is the normal force; p is the pore pressure.

$$\sigma_1 = \sigma_3 + \frac{2(c_s+\sigma_3\tan\varphi_s)}{(1-\tan\varphi_s\cot\beta_s)\sin 2\beta_s}, \tag{4}$$

where σ_1 is the compression strength; σ_3 is the confining pressure; β_s is the angle between the major principal stress and the normal direction of the structure plane.

2.2. Validation with the Theoretical Method. The results of the distribution of the abutment stress under the two typical bearing coal pillars illustrated in Figure 2 indicate that this numerical simulation model is more reliable than the theoretical model to predict the distribution of the abnormal stress. Both of theoretical calculation and numerical simulation results indicate the abnormal characteristics of the stress along both the vertical and horizontal direction. The stress contour line presents a similar distribution in shape. However, the results have something different in distribution, especially for the influence range. For example, the influence depth of the abutment stress contour line of 12 MPa is less than 15 meters for the theoretical calculation result while it reaches more than 17 meters for the numerical simulation results. This theoretical model was established under the hypothesis of the isotropous and homogeneous rock materials, which ignores the influences of the lithology difference and the structure plane between adjacent rock strata [3].

2.3. Validation with the Field Measuring Method. Field measuring method of decussation [34] was conducted to validate the reliability of the numerical simulation model in terms of the roof surface displacement of the underground

Table 3: Cap pressure of the double-yield model.

Number	1	2	3	4	5	6	7	8	9	10
Strain/mm/m	0.00	0.02	0.04	0.06	0.08	0.10	0.12	0.14	0.16	0.18
Stress/MPa	0.00	0.29	0.64	1.09	1.66	2.44	3.53	5.21	8.09	14.21

Table 4: Basic properties of the gob material.

Density (kg/m^3)	Bulk modulus (GPa)	Shear modulus (GPa)	Friction angle (°)	Dilation angle (°)
1200	5.56	2.27	8.96	6.28

Table 5: Structure plane properties used in the numerical model.

Shear stiffness (GPa/m)	Normal stiffness (GPa/m)	Friction angle (°)	Cohesion (MPa)	Tensile strength (MPa)
2	2	4.75	0.8	0.25

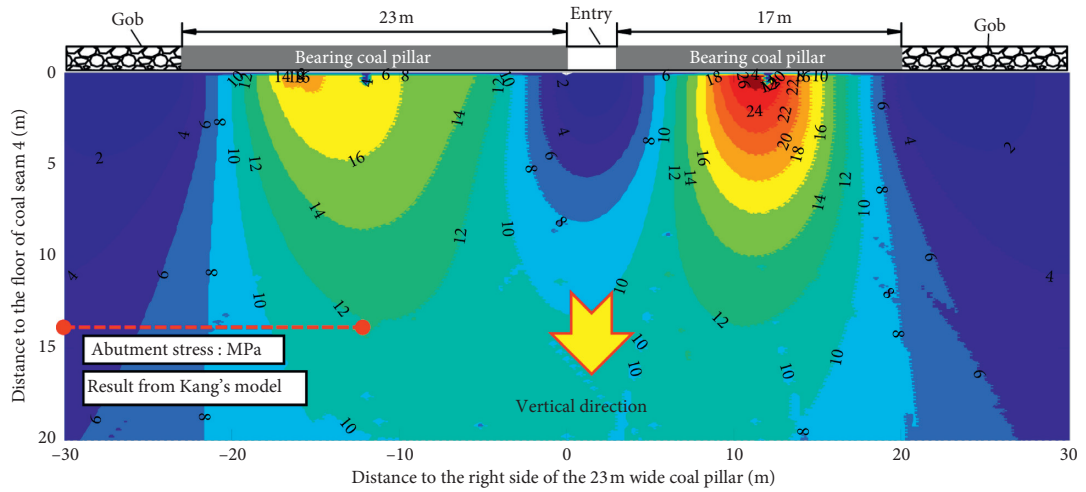

(a)

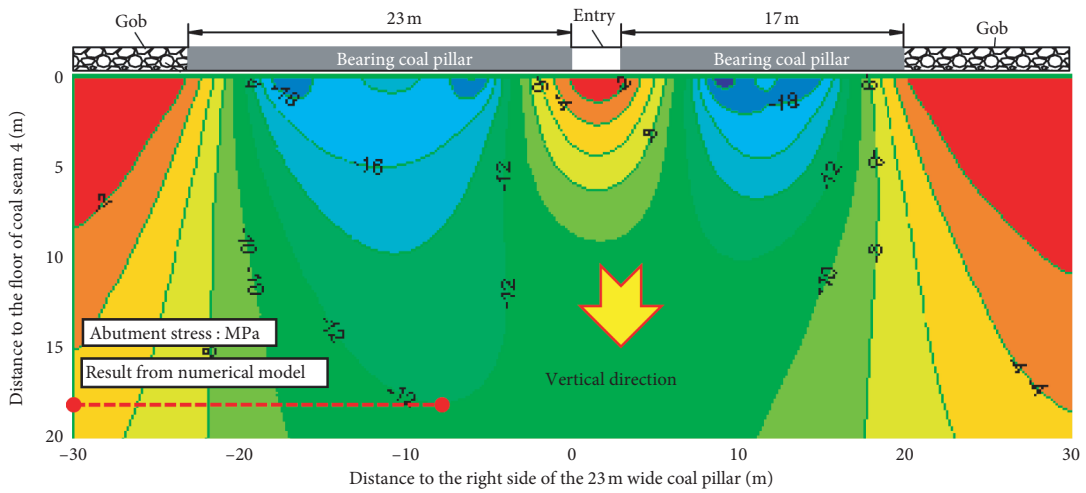

(b)

Figure 2: Distribution of the abutment stress under bearing coal pillars. (a) Theoretical calculation result; (b) numerical simulation result.

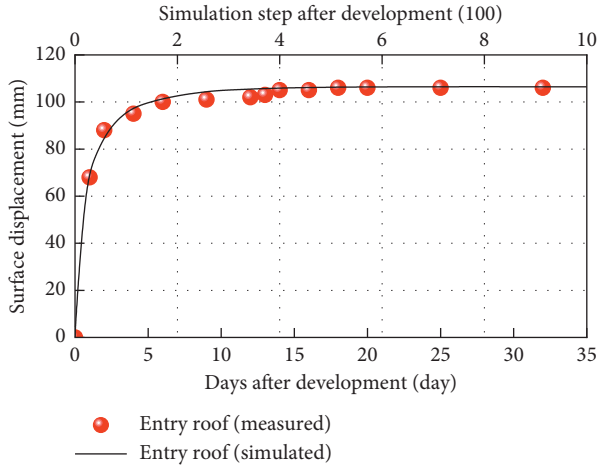

Figure 3: Comparison between the numerical simulation model and the field measuring method.

entry in coal seam 5. The results given in Figure 3 indicate that the numerical simulation model is reliable to predict the surface displacement of the entry roof since these results have a good agreement with each other. Actually, the surface displacement of underground space will present an increasing trend with the growth of the stress when the rock materials are determined [35]. The stress distribution, more reliable than the theoretical predicted result and the relative surface displacement of the entry consistent with the field measuring result together, demonstrated that the numerical simulation model is reliable to analyze the mechanical behavior of the coal and rock materials.

2.4. Simulation Plans of the Redistribution of Abnormal Stress. The numerical simulation process is divided into four steps to discover the redistribution of the abnormal stress under the bearing coal pillar to protect the underground space from large deformation. At the beginning, the three-dimensional numerical simulation model was established under the consideration of the geological and engineering conditions (Section 2.1). For the second step, the bearing coal pillars and gob material generalize by the mining operation in coal seam 4. The abnormal stress also generalizes in this step. Third, the mining entries including head entry and tail entry are established for the mining working face in coal seam 5 by the null model in FLAC3D software. Last but not least, the mining operation of the working face in coal seam 5 was carried out to calculate the redistribution of the abnormal stress.

Finding out the redistribution of the abnormal stress under bearing coal pillar with the retreating of the mining working face has a positive effect on the stability of the underground entry. Three indexes including stress concentration coefficient, stress gradient, and lateral pressure coefficient are determined to reveal the redistribution of the abnormal stress. Two typical areas are selected to layout the monitoring points including the area in front of the mining working face and the area in the side of the longwall panel as shown in Figure 4. And this bearing coal pillar is left in coal seam 4 while this mining working face is located in coal seam 5. This mining working face will pass across the coal below the bearing coal pillar. There are three monitoring points in front of the mining working face, which are arranged below the gob, the interaction of the bearing coal pillar and the stable gob, and the bearing coal pillar. The region of the interaction is determined in the zone where the stress concentration coefficient is less than 1 and the stress gradient is larger than 1. In addition, three monitoring lines are arranged in side of the longwall panel to record the redistribution of the abnormal stress in the side of the gob.

3. Results

3.1. Abnormal Stress in Front of the Mining Working Face

3.1.1. Stress Concentration Coefficient. The mining-induced redistribution of the stress concentration coefficient presents typical differences at different positions in front of the mining working face (Figure 5). It increases gradually with the approach of the mining working face, and its peak reaches 3.43 increasing by 50.44% compared with the starting value 2.28 in the point below the bearing coal pillar when the distance to the mining working face is less than 80 m. In the same time, it presents a similar increasing state with the decreasing of the distance to the mining working face, and the peak reaches 1.96, increasing by 96% compared with the starting value 1.00 in the point below the stable gob when the distance within 41 m. However, they are nearly kept stable and are less than 0.25 in the points below the interaction of the bearing coal pillar and the stable gob.

3.1.2. Stress Gradient. The mining-induced redistribution of the stress gradient is related to the distance from the mining working face and the relative location from the bearing coal pillar (Figure 6). It increases gradually and then reaches the peak value 1.20 MPa per meter increasing by 50% with the decrease of this distance for the area below the bearing coal pillar and the interaction of the bearing coal pillar and the stable gob when this distance is less than 80 m. In the same time, it increases relatively slowly for the area below the stable

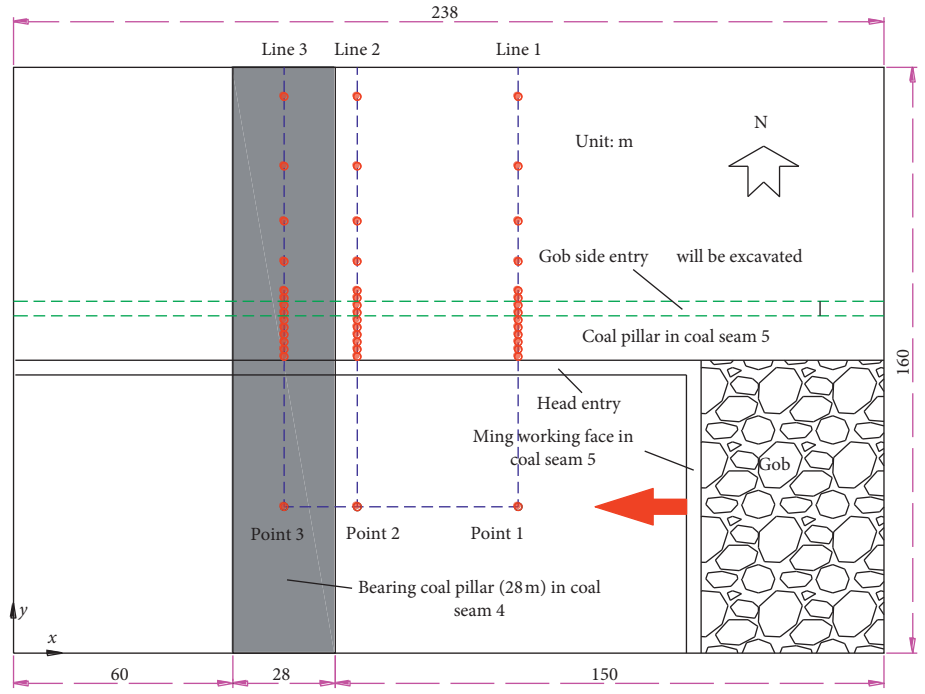

Figure 4: Monitoring scheme during the simulation step 4.

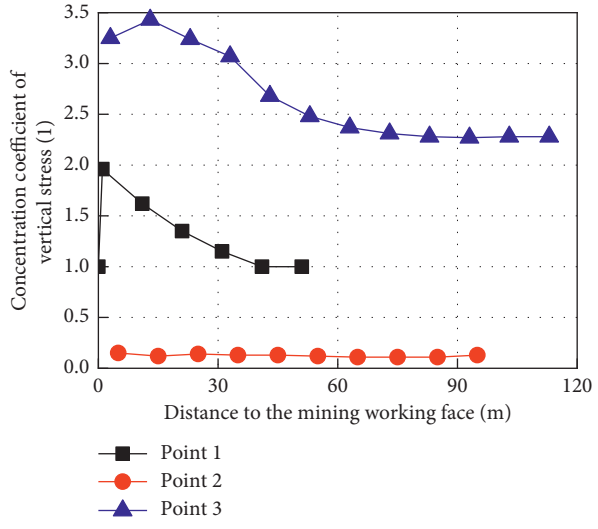

Figure 5: Concentration coefficient of abnormal stress in front of the mining working face.

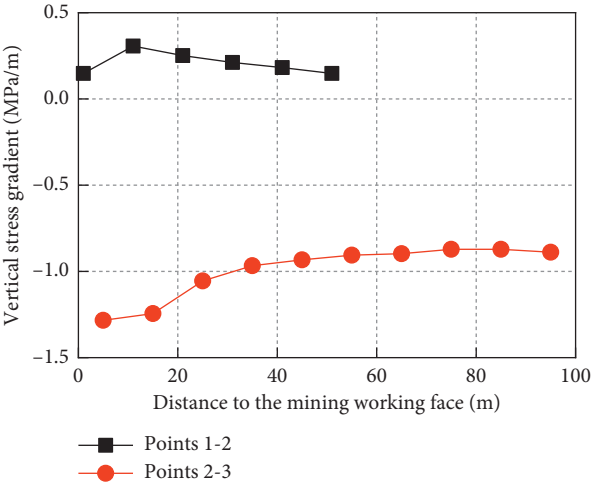

Figure 6: Stress gradient of abnormal stress in front of the mining working face.

gob with the maximum value of 0.31 MPa per meter and the growth rate of 107% when the distance is less than 50 m.

3.1.3. Lateral Pressure Coefficient. The mining-induced redistribution of the lateral pressure coefficient is influenced greatly by the distance to the mining working face (Figure 7). It decreases slowly in the area below the bearing coal pillar and the stable gob with the reduction of this distance when the distance is less than 80 m. However, it decreases first, increases slowly, then increases sharply to the peak, and finally decreases sharply in the area below the interaction of the bearing coal pillar and the stable gob with the reduction of the distance to the mining working face. The maximum reaches 7.6 increasing by 52%.

3.2. Abnormal Stress in Lateral of the Mining Working Face

3.2.1. Concentration Coefficient. The mining-induced redistribution of the stress concentration coefficient also presents typical differences at different positions in lateral of the mining working face (Figure 8). First, in the area below the stable gob, it increases linearly to the peak value and then decreases gradually to a stable value with the growth of the distance to the side rib of the head entry. This peak increases from 1.64 to 3.26, and the influence range increases from

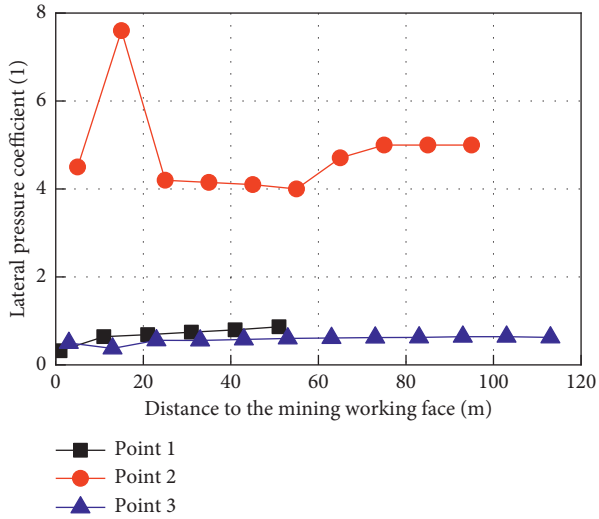

Figure 7: Lateral pressure coefficient of abnormal stress in front of the mining working face.

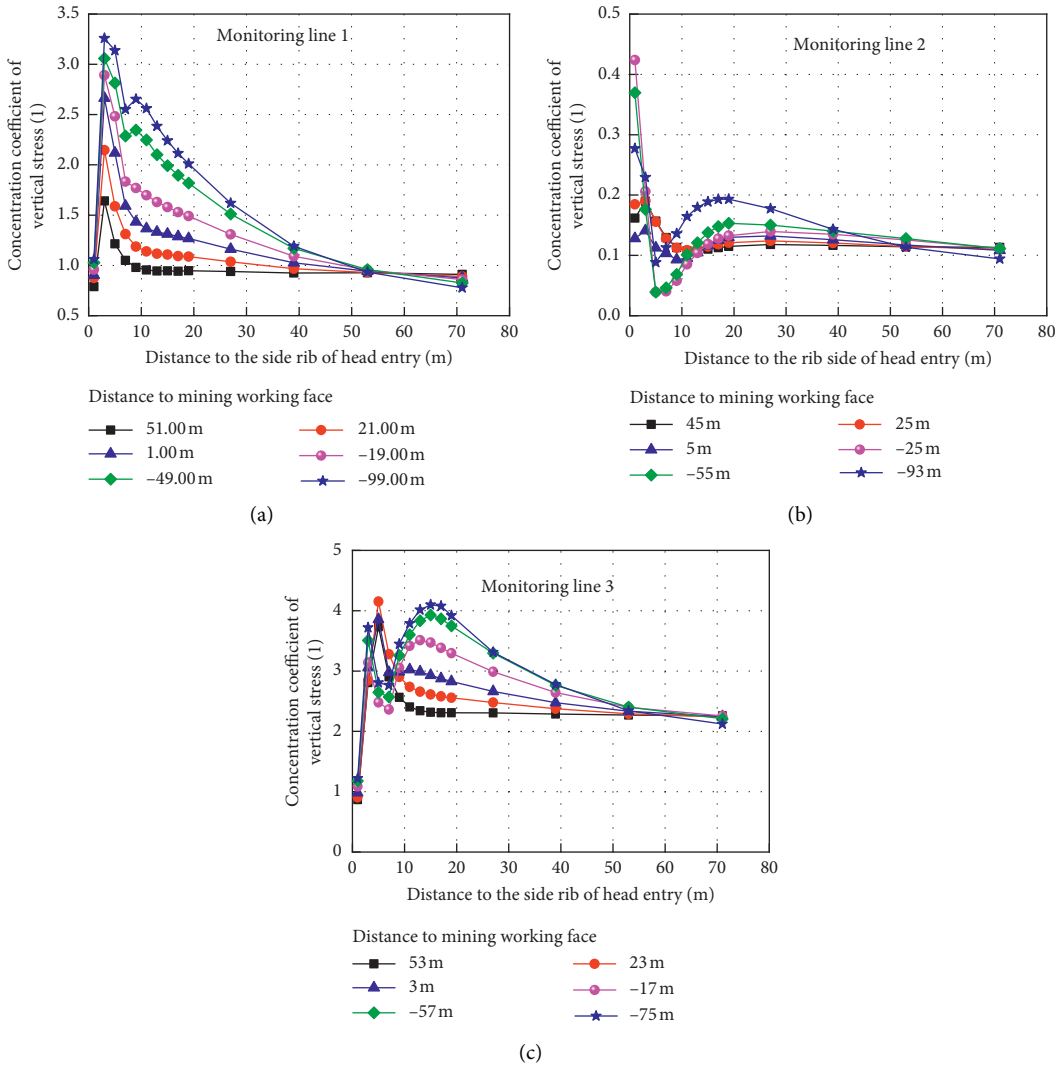

Figure 8: Concentration coefficient of abnormal stress in lateral of the mining working face. (a) Monitoring line 1, (b) monitoring line 2, and (c) monitoring line 3.

10 m to nearly 50 m with the reduction of the distance to the mining working face. Second, in the area below the interaction of the stable gob and the bearing coal pillar, it increases sharply to the peak value, decreases sharply to the valley, then increases gradually to the second peak, and finally decreases to a relatively stable value with the growth of the distance to the side rib of the head entry. The peak, second peak, and influence range increase from 0.19, 0.12, and 20 m to 0.42, 0.19, and 70 m, respectively, with the approach of the mining working face. Finally, in the area below the bearing coal pillar, it presents a similar variation to the concentration coefficient below the interaction area with the growth of the distance to the side rib of the head entry but differs in value and its change with the reduction of the distance to the mining working face. For example, the peak and second peak increase from 3.73 and 2.31 to 4.15 and 4.10, respectively, with the approach of the mining working face, which are very different from the values mentioned above.

3.2.2. Stress Gradient. The mining-induced redistribution of the stress gradient is related to the distance from the mining working face, the distance to the side rib of the head entry and the relative location from the bearing coal pillar (Figure 9). First, in the area below the stable gob, it decreases sharply to less than zero initially, increases closely to zero, then keeps stable or decreases slowly, and finally increases slowly close to zero again with the growth of the distance to the side rib of the head entry. The maximum of the variation amplitude reaches 5.04 MPa per meter with the approach of the mining working face. Second, in the area below the interaction of the bearing coal pillar and the stable gob, it is similar to that in the area below the bearing coal pillar in the variation trend with different values. For example, the maximum of the variation amplitude is just 0.92 MPa per meter with the approach of the mining working face. Finally, in the area below the bearing coal pillar, it also varies along the similar trend with that in the area below the stable gob but the values. For example, the maximum of the variation amplitude reaches 6.89 MPa per meter with the approaching of the mining working face.

3.2.3. Lateral Pressure Coefficient. The mining-induced redistribution of the lateral pressure coefficient is influenced greatly by the distance to the mining working face (Figure 10). It increases sharply initially, then decreases slowly, and finally increases gradually in the area below the stable gob with the distance to the side of the head entry. The maximum is 1.01, and the maximum of the amplitude is just 0.39 with the approach of the mining working face. In the area below the interaction of the bearing coal pillar and the stable gob, it presents a similar variation with that in the area below the stable gob, but it is much larger than that in the area below the stable gob. For example, the maximum reaches 10.00 and the maximum amplitude is 7.01 with the approach of the mining working face. However, in the area below the bearing coal pillar, it presents a very similar variation with that in the area below the stable gob, but it differs in values. The maximum is limited into 0.74 which is less than 1.00, and the maximum amplitude is 0.25.

4. Discussion

4.1. Contrastive Analysis. The mining effects on the abnormal stress under the bearing coal pillar mainly concentrate on the stress concentration coefficient, stress gradient, and lateral pressure coefficient in their values and influence ranges. These mechanical behaviors are induced from the superposition of the bearing coal pillar and the mining operations due to the fact that the mining effects on the area below the bearing coal pillar are prior to and more intense than those on other areas below the stable gob and the interaction. For example, compared with the initial values, the stress concentration coefficient increases by 0.96 in the area below the stable gob, 0.00 in the area below the interaction, and 1.15 in the area below the bearing coal pillar, and the influence range increases by 41 m, 0 m, and 80 m, respectively, in front of the mining working face.

In the same time, the mining disrupted strength is larger in the lateral side of the mining working face than that in front of the mining working face. For example, the stress concentration coefficient increases by 1.62 in the area below the stable gob, 0.23 in the area below the interaction, and 1.79 in the area below the bearing coal pillar, and the influence range increases by 40 m, 50 m, and 45 m, respectively, in the lateral side of the mining working face. Obviously, the stress concentration coefficient keeps less than 0.50 all the time with the influence of the mining operation. The mining-induced stress gradient has a similar variation with the stress concentration coefficient.

Differently, the lateral pressure coefficient has slight relationship with the mining operation in the areas below the stable gob and the bearing coal pillar but has strong relationship with the mining operation in the area below the interaction. For example, the lateral pressure coefficient increasing the amplitude reaches 6.38 in the area below the interaction, but it is 0.39 in the area below the stable gob and is 0.25 in the area below the bearing coal pillar. The main reason is because of the stress relief effects for the area below the interaction and stress reinforcement for the area below the bearing coal pillar and the stable gob during the mining operation.

4.2. Significance of the Results. The theoretical model can be used to predict the abnormal stress under the bearing coal pillar for the design of the entry layout without disturbing mining operation below this coal pillar [3]. However, this abnormal stress is forced to redistribute to a new condition influenced by the mining operation of the longwall face. Under the condition of the redistribution of the abnormal stress predicted by the numerical simulation model, four key problems including determination of the entry position, determination of the driving operation time, mining disturbing range warning, and prediction of the strengthening support area can be solved to protect the underground entry

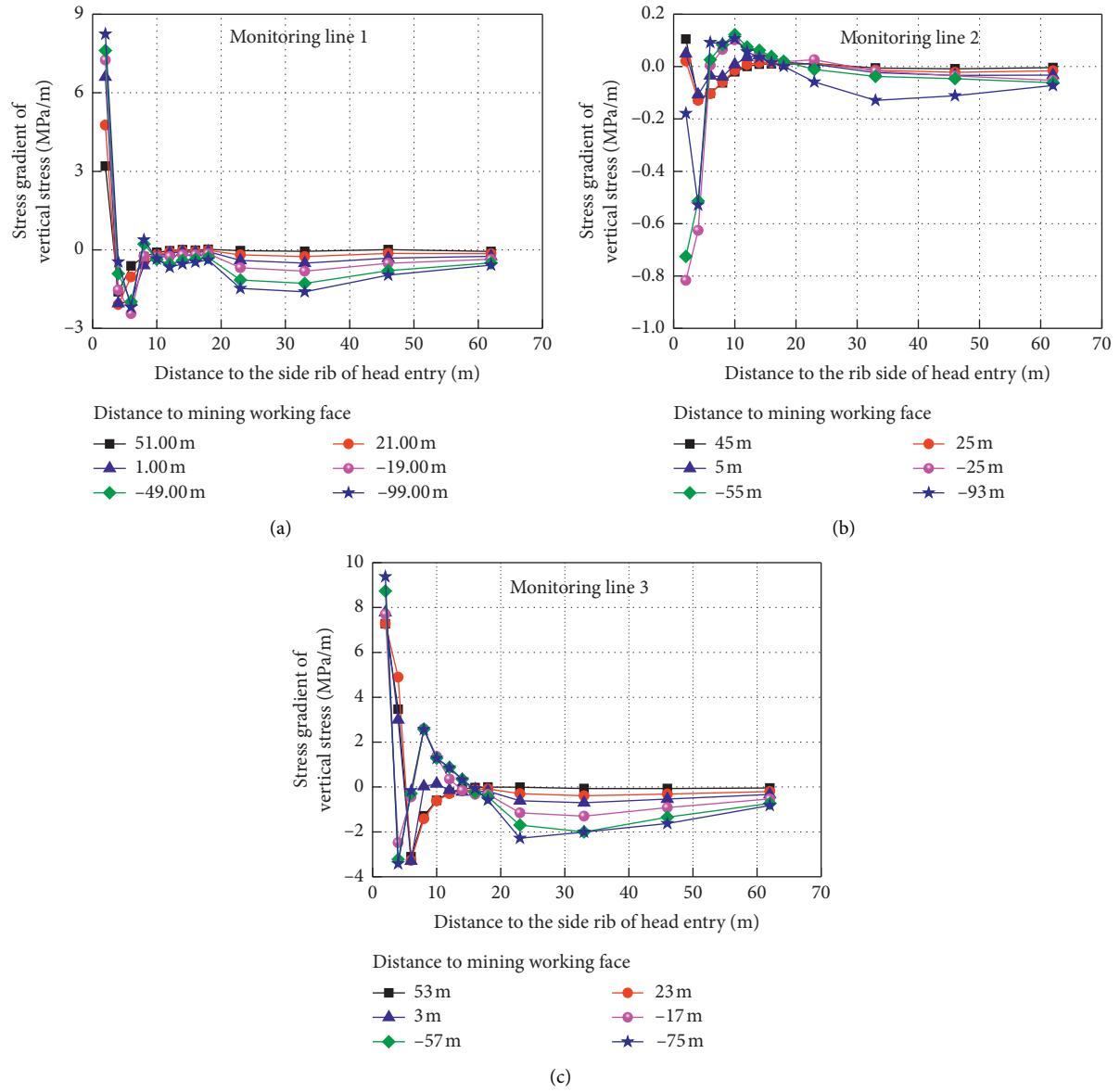

Figure 9: Stress gradient of abnormal stress in lateral of the mining working face. (a) Monitoring line 1, (b) monitoring line 2, and (c) monitoring line 3.

from mining-induced large deformation as shown in Figure 11.

The gob side entry under the bearing coal pillar can be layout at position I or position II with a coal pillar in coal seam 5. According to the typical judging criterion, this gob side entry should be arranged at position I where the stress concentration coefficient is less than 1 [36], and this position is determined as less than 2 m or more than 50 m away from the gob side rib. According to the judging criterion that the entry should layout in the zone where the stress concentration coefficient and the absolute value of the stress gradient are less than 1 and the lateral pressure coefficient is close to 1 [3], the position II can be determined at 50 m away from the gob side rib by the redistribution results of the abnormal stress.

If the gob side entry is excavated together with the head entry in the same time with a coal pillar, this entry system is called two-entry driving system [37]. Then, this gob side entry will suffer from the whole mining disturbing of the mining working face in coal seam 5. Determining the mining disturbing range has great significance to protect this kind of gob side entry. The numerical model results indicate that the mining disturbing range varies from 41 m in front of the mining working face to 99 m behind the mining working face in the area below the stable gob. While, it varies from 80 m in front of the mining working face to 75 m behind the mining working face in the area below the bearing coal pillar. For this warning area, the support of the gob side entry has to be strengthened to resist the influence of the mining disturbing.

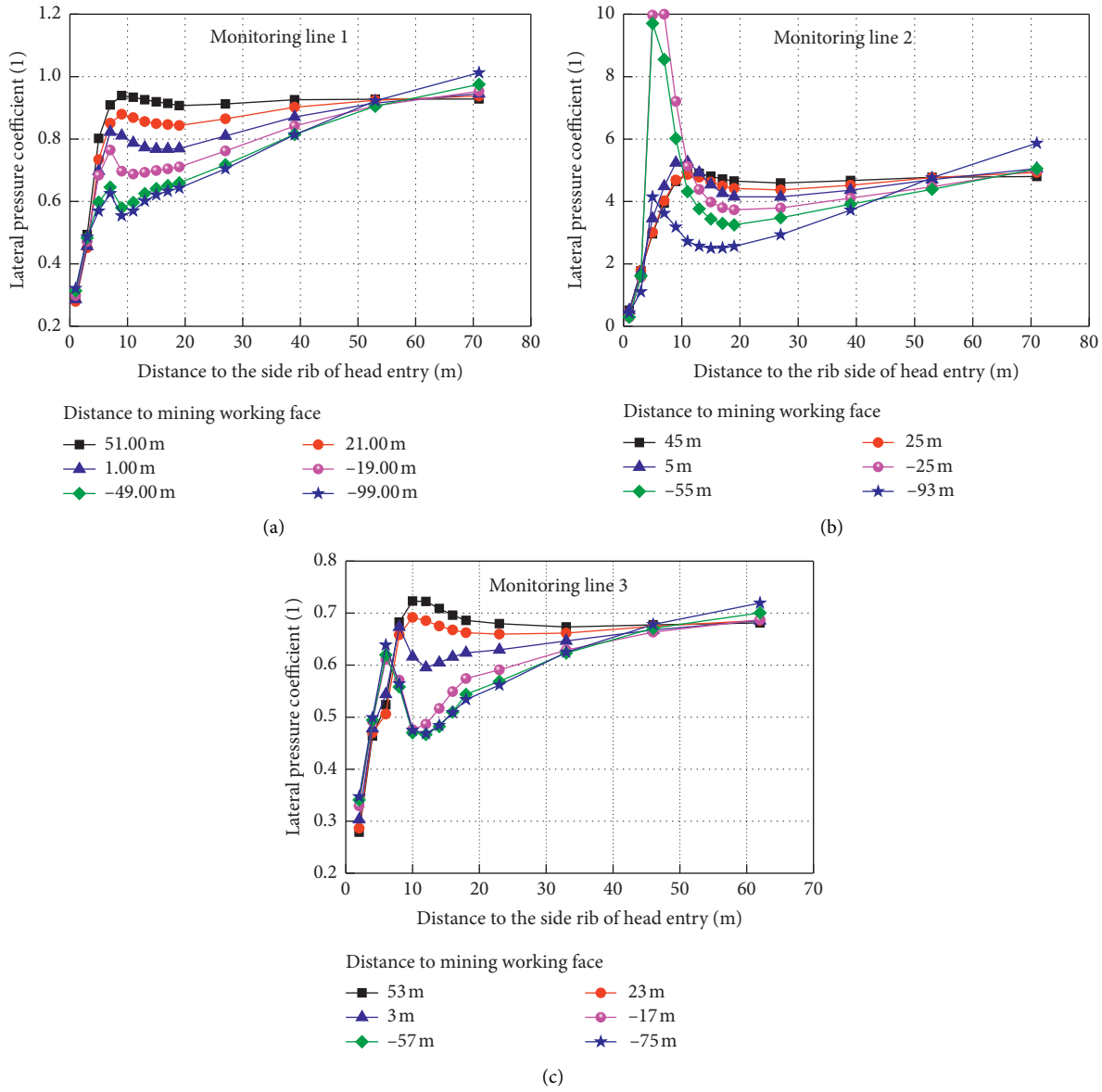

Figure 10: Lateral pressure coefficient of abnormal stress in lateral of the mining working face. (a) Monitoring line 1, (b) monitoring line 2, and (c) monitoring line 3.

If the gob side entry is excavated together with the retreating of the mining working face in coal seam 5, this entry system is called gob side entry driving heading adjacent to the advancing working face [38]. There are two key parameters to be determined before the driving operation of this gob side entry such as the driving stopping time and the driving starting time during this driving working face suffers from the mining disturbing. For example, the driving operation has to be stopped at 41 m in front of the mining working face and restart to drive at 99 m behind the mining working face in the area below the stable gob. While, the driving stopping time is determined as 80 m in front of the mining working face and the driving starting time is determined as 75 m behind the mining working face in the area below the bearing coal pillar.

4.3. Limitation of This Model. Though, in this numerical simulation model, the structure plane between the rock strata and the lithology differences of rock strata are considered to solve the limitation of the theoretical model, and this numerical simulation model has advantages to predict the mining-induced redistribution of the abnormal stress under the bearing coal pillar and ignores several problems. For example, the effects of the initial joints or cracks on the mechanical behaviors of the rock stratums and the mining-induced development of these joints or cracks are not considered. In addition, for some typical geological conditions, dynamic stress wave will generate from the hard roof fracture or caving, which cannot be ignored to layout the entry [39].

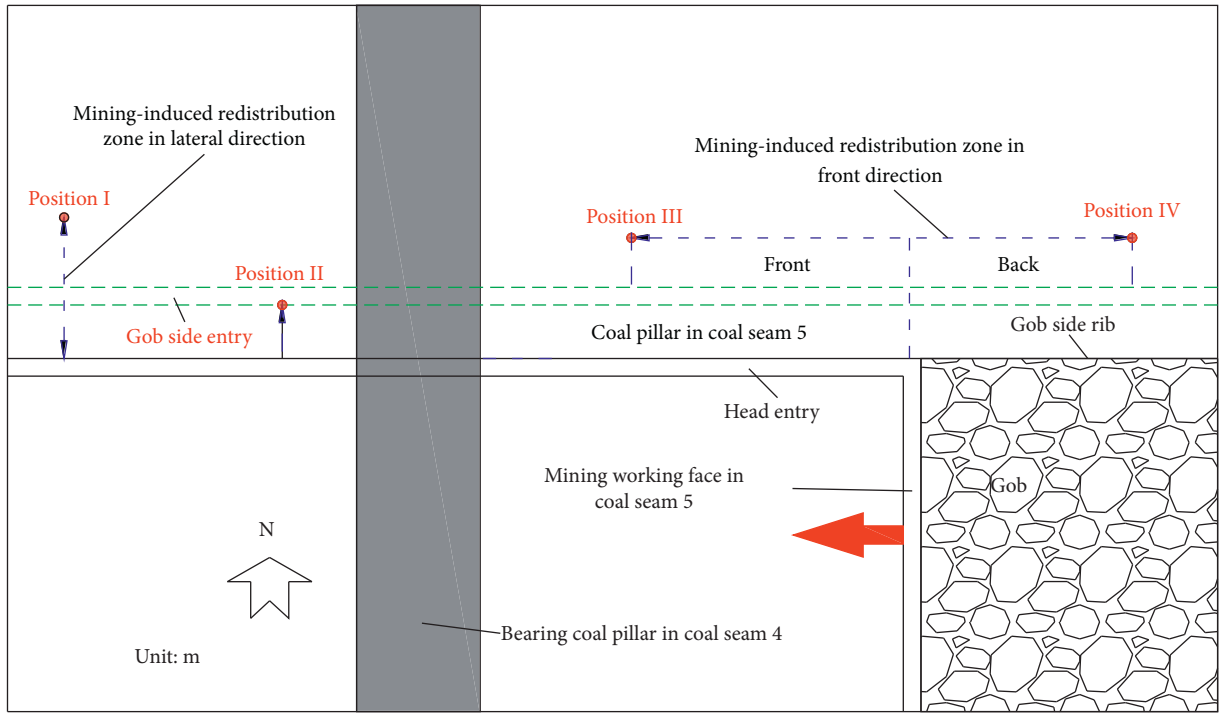

Figure 11: Key parameters to layout the entry under the bearing coal pillar.

5. Conclusion

The abnormal stress under the close bearing coal pillar plays a significant role in the control of the underground entry stability. A numerical simulation model was established to find out the mining-induced redistribution characteristics of this kind of abnormal stress. The double-yield model, the strain softening model, the interface model, and the Mohr–Coulomb model were determined to simulate the gob compaction effect, the pillar strength reduction effect, the structure plane discontinuity effect, and the rock mechanical behavior, respectively. This numerical mode was validated by comparing the abutment stress with the result of the theoretical method and surface displacement with the result of the measuring method.

The results of the validated numerical simulation model indicate that the mining operation mainly influence the stress concentration coefficient and stress gradient in the area below the bearing coal pillar and the stable gob and influence the lateral pressure coefficient in the area below the interaction of the bearing coal pillar and the stable gob. The stress concentration coefficient and stress gradient increase gradually and then decrease, and the lateral pressure coefficient decreases gradually, then increases, and finally decreases sharply with the approaching of the mining working face. Their maximum increasing rates are determined as 96%, 107%, and 52%, respectively, in front of the mining working face. In the same time, they are 121.05%, 198.56%, and 236.82%, respectively, in the lateral side of the mining working face.

The predicted mining-induced redistribution of the abnormal stress is available for designing the underground entry layout under the bearing coal pillar with disturbance of the mining operation. The gob side entry has to be excavated at more than 50 m away from the gob side rib. The gob side entry support has to be strengthened in the area from 80 m in front of the mining working face to 99 m behind the mining working face in the two-entry driving system. Gob side entry driving heading adjacent to the advancing working face also has to stop at 80 m in front of the mining working face and restart at 90 m behind the mining working face.

Data Availability

The data used to support the findings of this study are included within the article.

Conflicts of Interest

The authors declare that they have no conflicts of interest.

Acknowledgments

This work was supported by the National Natural Science Foundation of China (51804099 and 52074239), the Focus Research and Special Development for Scientific and Technological Project of Henan province (202102310542), the Fundamental Research Funds of the Central Universities (2017CXNL01), the Key Scientific Research Project Fund of Colleges and Universities of Henan Province (19A440011), and the Fundamental Research Funds for the Universities of Henan Province (NSFRF180328).

References

[1] M. G. Qian, P. W. Shi, and J. L. Xu, *Mining Pressure and Strata Control*, China University of Mining and Technology Press, Xuzhou, China, 2nd edition, 2010.

[2] Y. Li, Y. Ren, S. S. Peng, H. Chen, N. Wang, and J. Luo, "Measurement of overburden failure zones in close-multiple coal seams mining," *International Journal of Mining Science and Technology*, vol. 31, no. 1, pp. 43–50, 2020.

[3] J. Kang, W. Shen, J. Bai et al., "Influence of abnormal stress under a residual bearing coal pillar on the stability of a mine entry," *International Journal of Mining Science and Technology*, vol. 27, no. 6, pp. 945–954, 2017.

[4] S. Lu, Y. Jiang, and Y. Sun, "The selection of vertical distance Z between roadway and its upper coal seam," *Journal of China University of Mining and Technolgy*, vol. 22, no. 1, pp. 4–10, 1993.

[5] Z. Sun, Y. Wu, Z. Lu, Y. Feng, X. Chu, and K. Yi, "Stability analysis and derived control measures for rock surrounding a roadway in a lower coal seam under concentrated stress of a coal pillar," *Shock and Vibration*, vol. 2020, Article ID 6624983, 12 pages, 2020.

[6] X. Wang, J. Bai, W. Li, B. Chen, and V. D. Dao, "Evaluating the coal bump potential for gateroad design in multiple-seam longwall mining: a case study," *Journal of the Southern African Institute of Mining and Metallurgy*, vol. 115, no. 8, pp. 755–760, 2015.

[7] J.-X. Yang, C.-Y. Liu, B. Yu, and F.-F. Wu, "Calculation and analysis of stress in strata under gob pillars," *Journal of Central South University*, vol. 22, no. 3, pp. 1026–1036, 2015.

[8] W. Ru, S. Hu, J. Ning et al., "Study on the rheological failure mechanism of weakly cemented soft rock roadway during the mining of close-distance coal seams: a case study," *Advances in Civil Engineering*, vol. 2020, Article ID 8885849, 20 pages, 2020.

[9] H. Yang, Z. Guo, D. Chen, C. Wang, F. Zhang, and Z. Du, "Study on reasonable roadway position of working face under strip coal pillar in rock burst mine," *Shock and Vibration*, vol. 2020, Article ID 8832791, 21 pages, 2020.

[10] D. Chen, E. Wang, S. Xie et al., "Roadway surrounding rock under multi-coal-seam mining: deviatoric stress evolution and control technology," *Advances in Civil Engineering*, vol. 2020, Article ID 9891825, 18 pages, 2020.

[11] G. Wu, X. Fang, H. Bai, M. Liang, and X. Hu, "Optimization of roadway layout in ultra-close coal seams: a case study," *PLoS One*, vol. 13, no. 11, pp. 1–14, 2018.

[12] H. Shang, J. Ning, S. Hu, S. Yang, and P. Qiu, "Field and numerical investigations of gateroad system failure under an irregular residual coal pillar in close-distance coal seams," *Energy Science & Engineering*, vol. 7, no. 6, pp. 2720–2740, 2019.

[13] S. Lu, Y. Sun, and Y. Jiang, "Selection of horizontal distance X between roadway and the edge of its upper pillar," *Journal of China University of Mining and Technology*, vol. 23, no. 1, pp. 43–51, 1994.

[14] L. Xinjie, L. Xiaomeng, and P. Weidong, "Analysis on the floor stress distribution and roadway position in the close distance coal seams," *Arabian Journal of Geosciences*, vol. 9, no. 2, p. 83, 2016.

[15] X. Gao, S. Zhang, Y. Zi, and S.-K. Pathan, "Study on optimum layout of roadway in close coal seam," *Arabian Journal of Geosciences*, vol. 13, no. 15, p. 746, 2020.

[16] Z. Zhang, M. Deng, X. Wang, W. Yu, F. Zhang, and V. Dao, "Field and numerical investigations on the lower coal seam entry failure analysis under the remnant pillar," *Engineering Failure Analysis*, vol. 115, p. 104638, 2020.

[17] Z. Zhang, H. Shimada, D. Qian, and T. Sasaoka, "Application of the retained gob-side gateroad in a deep underground coalmine," *International Journal of Mining, Reclamation and Environment*, vol. 30, no. 5, pp. 371–389, 2016.

[18] J.-B. Bai, W.-L. Shen, G.-L. Guo, X.-Y. Wang, and Y. Yu, "Roof deformation, failure characteristics, and preventive techniques of gob-side entry driving heading adjacent to the advancing working face," *Rock Mechanics and Rock Engineering*, vol. 48, no. 6, pp. 2447–2458, 2015.

[19] J. F. Labuz and A. Zang, "Mohr-coulomb failure criterion," *Rock Mechanics and Rock Engineering*, vol. 45, no. 6, pp. 975–979, 2012.

[20] F. Wu, B. Chen, Q. Zou et al., "Range estimation of horizontal stress of deep rock based on Mohr-Coulomb criterion," *Results in Physics*, vol. 12, pp. 2107–2111, 2019.

[21] C. J. Hou and N. J. Ma, "Stress in in-seam roadway sides and limit equilibrium zone," *Journal of China Coal Society*, vol. 4, pp. 21–29, 1989.

[22] X. Wang, J. Bai, R. Wang, and W. Sheng, "Bearing characteristics of coal pillars based on modified limit equilibrium theory," *International Journal of Mining Science and Technology*, vol. 25, no. 6, pp. 943–947, 2015.

[23] E. Esterhuizen, C. Mark, and M. M. Murphy, "Numerical model calibration for simulating coal pillars, gob and overburden response," in *Proceedings of the Twenty-Ninth International Conference on Ground Control in Mining*, Morgantown, WV, USA, January 2010.

[24] W. Li, J. Bai, S. Peng, X. Wang, and Y. Xu, "Numerical modeling for yield pillar design: a case study," *Rock Mechanics and Rock Engineering*, vol. 48, no. 1, pp. 305–318, 2015.

[25] W. Shen, G. Shi, M. Wang et al., "Method of entry layout under synergistic effects of abutment stress and dynamic stress," *Shock and Vibration*, vol. 2020, Article ID 6655293, 16 pages, 2020.

[26] S. Liu, X. Li, D. Wang, and D. Zhang, "Experimental study on temperature response of different ranks of coal to liquid nitrogen soaking," *Natural Resources Research*, vol. 30, no. 2, pp. 1467–1480, 2021.

[27] X. Zhang, J. Hu, H. Xue et al., "Innovative approach based on roof cutting by energy-gathering blasting for protecting roadways in coal mines," *Tunnelling and Underground Space Technology*, vol. 99, p. 103387, 2020.

[28] M. Shabanimashcool and C. Li, "Numerical modelling of longwall mining and stability analysis of the gates in a coal mine," *International Journal of Rock Mechanics and Mining Sciences*, vol. 51, pp. 24–34, 2012.

[29] M. Salamon, "Mechanism of caving in longwall coal mining, presented at the in: rock mechanics contribution and challenges," in *Proceedings of the 31st US Symposium of Rock Mechanics*, Golden, CO, USA, 1990.

[30] Y. J. Zhang, S. J. Liu, M. M. Kou, and Z. Q. Wang, "Mechanical and failure characteristics of fissured marble specimens under true triaxial compression: insights from 3-D numerical simulations," *Computers and Geotechnics*, vol. 127, Article ID 103785, 2020.

[31] W.-L. Shen, J.-B. Bai, W.-F. Li, and X.-Y. Wang, "Prediction of relative displacement for entry roof with weak plane under the effect of mining abutment stress," *Tunnelling and Underground Space Technology*, vol. 71, pp. 309–317, 2018.

[32] F. D. Itasca, *Fast Lagrangian Analysis of Continua in 3 Dimensions*, Itasca Consulting Group, Minneapolis, MN, USA, 2012.

[33] J. C. Jaeger and N. Cook, *Fundamentals of Rock Mechanics*, Wiley, vol. 93, Hoboken, NJ, USA, Fourth edition, 1979.
[34] W. Shen, T. Xiao, M. Wang, J. Bai, and X. Wang, "Numerical modeling of entry position design: a field case," *International Journal of Mining Science and Technology*, vol. 28, no. 6, pp. 985–990, 2018.
[35] V. Kontogianni and S. Stiros, "Induced deformation during tunnel excavation: evidence from geodetic monitoring," *Engineering Geology*, vol. 79, pp. 115–126, 2005.
[36] C. J. Hou, *Roadway Surrounding Rock Control*, China University of Mining and Technology Press, Xuzhou, Jiangsu, China, 2013.
[37] W.-L. Shen, W.-B. Guo, H. Nan, C. Wang, Y. Tan, and F.-Q. Su, "Experiment on mine ground pressure of stiff coal-pillar entry retaining under the activation condition of hard roof," *Advances in Civil Engineering*, vol. 2018, Article ID 2629871, 11 pages, 2018.
[38] G. Zhang, C. Zang, M. Chen, G. Tao, and D. Zhao, "Ground response of entries driven adjacent to a retreating longwall panel," *International Journal of Rock Mechanics and Mining Sciences*, vol. 138, Article ID 104630, 2021.
[39] X. Li, Z. Cao, and Y. Xu, "Characteristics and trends of coal mine safety development," *Energy Sources, Part A: Recovery, Utilization, and Environmental Effects*, 2020.